J. Adv. Model. Earth Syst., **Vol. 3**, Art. 2011MS000079, 14 pp.

Convective quasi-equilibrium reconsidered

David J. Raymond and Michael J. Herman

Physics Department and Geophysical Research Center, New Mexico Institute of Mining and Technology, Socorro, New Mexico, USA

Manuscript submitted 19 April 2011

The hypothesis of convective quasi-equilibrium states that moist convection reacts almost instantly to drive the atmospheric temperature profile throughout the troposphere to one of a special subset of possible profiles. In a simple case this might consist of a moist adiabat with the saturated moist entropy of the adiabat equaling the moist entropy of the boundary layer. In more complex cases the target temperature profile might depend on the moisture profile as well as boundary layer conditions. We present evidence from analytical and numerical calculations which challenge the validity of this hypothesis. These calculations involve both a simple, physically based parameterization of the effects of convection on its environment and a complex cloud-resolving model. In both cases we show that imposed temperature perturbations in the lower troposphere are rapidly eliminated, while those in the upper troposphere are not. The rapid temperature relaxation in the lower troposphere is due to the near-instantaneous change in the precipitation rate and latent heat release provoked by the temperature anomaly. Water vapor is so limited in the upper troposphere that this process cannot act there.

DOI:10.1029/2011MS000079

1. Introduction

The notion of convective quasi-equilibrium (CQE) has dominated thinking about the interaction between deep moist convection and the environment for at least two decades. In this view the time scale for convection to remove a buoyancy perturbation at any level in the atmosphere reached by the convection is of order the time required for a convective cell to pass through its life cycle, i.e., a few hours. Such a time scale seems plausible by analogy with dry atmospheric convection in the boundary layer, where convective instability results in an immediate convective response.

The implementation of this idea takes numerous forms, but is perhaps most elegantly expressed by *Emanuel et al.* [1994, hereinafter ENB]. In their paper convection is postulated to relax the atmosphere rapidly to one of a particular family of profiles (in the simplest case a moist adiabat), with the choice of profile being related solely to the boundary layer moist entropy. The boundary layer moist entropy (over the ocean) in turn is a function of the sea surface temperature (SST), the surface wind speed, and the large-scale vertical motion. Strong ascent is associated with more convection, and hence a stronger downdraft flux into the boundary layer, which tends to reduce the boundary layer entropy. High SST and strong winds tend to increase the entropy, and the actual boundary layer entropy is a balance between these competing tendencies. The reduction in entropy and the corresponding shift to a cooler target moist adiabat where there is large-scale ascent compresses all the complexity of moist convection into an "effective static stability" which is of order 10% of the dry static stability of the troposphere.

Though ENB is the most coherent and complete statement of the principle of CQE, a number of models incorporating this idea in one form or another predate ENB by as much as three decades. A notable model employing CQE is the convective parameterization of *Arakawa and Schubert* [1974]. In their model, the "cloud work function" of each member of an ensemble of convective plumes with different entrainment rates is assumed to change only slowly with time. (The cloud work function is a kind of convective available potential energy (CAPE) which takes into account the effects of entrainment.) Thus, strong tendencies in the environmental profile are instantly compensated by rapid changes in the mass fluxes associated with each ensemble member so as to keep the associated cloud work functions

To whom correspondence should be addressed.
M. J. Herman and D. J. Raymond, Physics Department, New Mexico Institute of Mining and Technology, Socorro, NM 87801, USA
raymond@kestrel.nmt.edu

nearly constant. The result is a CQE model with rapid relaxation to a target temperature profile which is a function of other aspects of the environment, particularly the humidity profile.

Variations on the original Arakawa-Schubert scheme include a "relaxed" scheme in which instantaneous adjustment is replaced by a relaxation to the adjusted state [*Moorthi and Suarez*, 1992; *Randall and Pan*, 1993; *Pan and Randall*, 1998], the introduction of improved cloud physics [*Sud and Walker*, 1999a, 1999b], and a scheme in which a minimum entrainment rate is imposed on convective plumes [*Tokioka et al.*, 1988]. With the possible exception of Tokioka's modification, these changes are unlikely to affect the quasi-equilibrium character of the parameterization.

Another widely used convective parameterization based on CQE is that of Betts and Miller [*Betts*, 1986; *Betts and Miller*, 1986, 1993]. This adjustment scheme exhibits rapid relaxation to a one-dimensional family of reference profiles as advocated by ENB.

The linearized model of *Neelin and Yu* [1994] illustrates the dynamical consequences of convective quasi-equilibrium theory. (See *Raymond et al.* [2009] for a simplified presentation of the Neelin-Yu model.) This model utilizes a simplified version of the Betts-Miller parameterization. The most interesting large-scale, convectively coupled modes in this model are waves with first baroclinic mode vertical structure but propagation speeds reduced from those of adiabatic gravity waves with the same vertical structure. The reduction factor is proportional to the square root of the gross moist stability [*Neelin and Held*, 1987; see also *Raymond et al.*, 2009] a concept related to ENB's effective static stability. Given the postulated value of this reduction factor, the waves move at roughly the observed speed of convectively coupled equatorial Kelvin waves. With no air-sea interactions, these modes are weakly decaying as a result of the assumed 1–2 hr lag between convective forcing and the convective response. *Neelin and Yu* [1994] indicate that surface latent heat flux perturbations associated with wave-generated wind perturbations in the presence of a mean wind destabilize such waves. Convectively coupled modes with vertical structure of shorter vertical wavelength decay strongly due to the rapid dissipation of their vertical structure implied by the CQE hypothesis.

The global circulation model of *Frierson* [2007] also uses a simplified Betts-Miller scheme, and equatorial Kelvin waves produced by this model likewise show propagation speeds proportional to the square root of the gross moist stability. Temperature and zonal wind perturbations in these simulated Kelvin waves exhibit first baroclinic mode structure, as expected from characteristics of a convective parameterization based on CQE.

The non-tilted structure of Kelvin waves produced by simple quasi-equilibrium parameterizations such as Betts-Miller is in disagreement with observations. As *Straub and Kiladis* [2002], *Majda and Biello* [2004], *Yang et al.* [2007], and *Kiladis et al.* [2009] show, the temperature and zonal wind perturbation structures of observed convectively coupled Kelvin waves exhibit a westward tilt from the surface to the middle to upper troposphere and an eastward tilt above this level. This suggests a fundamental difficulty with at least simple CQE theories, which drive the atmosphere to a first baroclinic mode temperature structure on very short time scales, and thus do not admit solutions with tilted temperature perturbations. (Technically, virtual temperature should be used to derive the phase structure of observed waves, but we have verified that the use of temperature rather than virtual temperature introduces systematic errors in the virtual temperature perturbation pattern of at most 10–15% at any given level.) The Arakawa-Schubert model as modified by *Tokioka et al.* [1988] results in some tilted structure [*Lee et al.*, 2003; *Frierson et al.*, 2011]; this could be related to the suppression of convection with small entrainment rates implemented in this modification, which likely frustrates the rapid adjustment associated with CQE.

Arakawa and Schubert [1974] argued for the validity of tropospheric quasi-equilibrium by showing that the observed time rate of change of the work function in the tropical west Pacific is much less than the tendency of the work function due to large-scale processes there. However, *Yano et al.* [2000] showed that the interpretation of this result is ambiguous, and could be explained by other factors not related to the rapidity with which convection eliminates convective instability. Furthermore, *Zhang* [2002] showed in a middle latitude land area that the total tendency of CAPE is comparable to the large-scale tendency of CAPE, so that the CQE assumption is not valid there.

So far the discussion has been limited to full tropospheric quasi-equilibrium in which all levels reached by convection, including the boundary layer, undergo rapid adjustment to a reference profile. *Raymond* [1995] and *Emanuel* [1995] proposed a different type of statistical equilibrium called boundary layer quasi-equilibrium (BLQ), in which the increase in boundary layer moist entropy due to surface fluxes is in balance with the tendency of moist downdrafts to decrease the entropy. This model is thus a quasi-equilibrium theory of the control of convection by convective inhibition (CIN). If the character of the resulting convection (mass and moisture flux profiles, etc.) can be related to the environmental profiles of wind, temperature, and humidity, the theory becomes a closed model of convective forcing.

Mapes [2000] developed a simplified model of convectively coupled tropical waves based on the idea that deep convection is forced when eddy kinetic energy in the boundary layer is sufficient to overcome CIN. This is a non-equilibrium theory of CIN control of convection, and Mapes suggests that the non-equilibrium aspect of his theory is important.

A series of models related to that of *Mapes* [2000] has recently appeared in the literature of, e.g., *Majda and Shefter* [2001], *Khouider and Majda* [2006], *Raymond and Fuchs* [2007], *Kuang* [2008a, 2008b], and *Khouider and Majda* [2008]. Many of these invoke a "lower troposphere quasi-equilibrium" in their treatment of cumulus convection which is similar to the full tropospheric quasi-equilibrium of ENB, but is applied only to the lower part of the troposphere.

Kuang [2008a] in particular has justified simplified models of this type on the basis of a cloud-resolving model of convection which is coupled to a single large-scale Fourier mode representative of a convectively coupled wave. Such models are able to reproduce the observed tilted structure of convectively coupled equatorial Kelvin waves. Adjustment of the atmosphere to boundary layer changes occurs on convective time scales only in the lower troposphere in this model.

Kuang [2010] confirmed the above results in a series of numerical experiments testing the response of convection in a cloud-resolving model to moisture and temperature perturbations. A clever numerical technique was used in these experiments, in which the moisture and temperature perturbations were actually produced by a set of imposed moisture and temperature tendencies. Tendency amplitudes were kept small enough to make the relationship between the tendencies and perturbations linear, thus allowing the relationship between the two to be represented by a linear transformation. The resulting matrix was then inverted to obtain the tendencies resulting from the perturbations. The eigenvalues and eigenvectors of the inverted matrix were also calculated. Physically, the eigenvectors represent profiles of temperature and moisture perturbations which decay as a result of convective activity without changing shape. The eigenvalue in each case is the decay rate of the corresponding eigenvector profile. As in the earlier work, the time scale for the convection to eliminate temperature and moisture perturbations is much greater in the upper troposphere than at lower levels.

Kuang [2010] and *Tulich and Mapes* [2010] also made forward calculations in which the response to temperature and moisture perturbations in a cloud-resolving model was computed directly. In particular, the decay of moisture and temperature perturbations imposed on the lower troposphere was more rapid than for similar perturbations imposed at middle levels. *Kuang* [2010] found good agreement between his forward and inverse calculations.

Given the questions raised above about full tropospheric CQE, we reexamine the theoretical underpinnings of the CQE hypothesis. We start in section 2 with a description of a toy convective parameterization and a discussion of two diagnostics pertaining to this study. In section 3 the toy convective scheme is run in a single-column model in which the response to perturbations in temperature from radiative-convective equilibrium (RCE) are explored. The same exercise is then done with a cloud-resolving model in section 4. These calculations were performed in a manner similar to those of *Tulich and Mapes* [2010]. As with *Tulich and Mapes* [2010] and *Kuang* [2010], both of these tests indicate that lower tropospheric temperature and humidity perturbations elicit a rapid response from convection and convective rainfall, while upper tropospheric temperature perturbations result in a much slower response.

2. Toy Model of Convection

The cumulus parameterization of *Raymond* [2007] is an adjustment scheme in the sense that profiles of moist entropy (or equivalent potential temperature) and total cloud water mixing ratio (vapor plus advected condensate) undergo conservative relaxation toward profiles constant in height through the depth of the convection. In the absence of other effects, this results ultimately in profiles well mixed in cloud water mixing ratio with moist adiabatic temperature profiles where saturation occurs and dry adiabatic profiles in unsaturated regions. However, processes including radiative heating and cooling, precipitation production and evaporation, and the instantaneous distribution of surface moist entropy and water vapor fluxes through the depth of the convective layer intervene to keep this from happening.

Two modes of the model are run in parallel at each grid point, one in which the depth of the convection is that of the ultimate level of neutral buoyancy of planetary boundary layer (PBL) parcels (excluding minor layers of negative buoyancy), and the other in which the convective layer is the PBL itself. The actual tendencies are taken to be a weighted average of the deep and PBL tendencies, with greater convective inhibition favoring the PBL mode.

Two crucial time scales act in this parameterization, the time scale for the adjustment of moist entropy and that for the depletion of cloud water by precipitation [see also *Tompkins and Craig*, 1998]. A simplified definition of moist entropy is

$$s = C_p \ln\theta + Lr/T_R, \tag{1}$$

where θ is the potential temperature, r is the water vapor mixing ratio, C_p is the specific heat of air at constant pressure, L is the (constant) latent heat of condensation, and T_R is a constant reference temperature. We define an additional variable, the adiabatic warming

$$j = C_p \ln\theta - Lr/T_R. \tag{2}$$

Latent heat release increases θ and decreases r in such a way that the moist entropy s remains constant. In contrast such latent heat release increases the adiabatic warming as a result of the changes in both θ and r. ("Adiabatic" refers to moist adiabatic in this case.) Thus, j responds rapidly to condensation and the production of precipitation, whereas s is not affected by these processes and changes more slowly

via the weaker mechanisms of radiative heating and cooling and surface heat fluxes.

In subsequent sections we perturb RCE temperature profiles in the upper and lower troposphere in a single column model involving our toy cumulus parameterization and in a cloud-resolving model, and examine how rapidly the convection returns the temperature profile to radiative-convective equilibrium in each case. This restoration is expressed most conveniently by the time evolution of the column-averaged moist entropy and adiabatic warming as well as the evolution of the precipitation rate. By this analysis we obtain the response of both the potential temperature and mixing ratio to the initial perturbation. However, by expressing the result in terms of s and j we separate the response's slow and fast components.

Convection in physically realistic RCE cases is typically quite sparse. We emulate stronger convection while maintaining the simplicity of RCE by simultaneously increasing the radiative cooling and the surface exchange coefficients. In this way we can examine how the response characteristics of convection change with the strength of convection while avoiding the complexity of non-RCE calculations.

3. Impulsive Heating in a Single-Column Toy Model

To investigate how the single-column toy model of convection (SCM) adjusts to warm and cold anomalies at different elevations, perturbations are applied to an RCE base state. The model uses a simple, fixed radiative cooling profile that is constant below 12 km with a linear decrease to zero near the tropopause (15 km) above this level. Surface fluxes are proportional to the surface wind and are determined using a bulk flux scheme, so that the model forcing is completely defined by the SST (assumed constant), the magnitude of the drag coefficient, and the tropospheric radiative cooling rate. In order to examine the sensitivity of this experiment to variations in convective activity, we vary the latter two parameters over a series of trials (see Table 1).

Moist radiative-convective equilibrium is the quasi-steady state of the atmosphere wherein the outgoing vertical radiative flux of entropy at the top of the atmosphere is balanced by the vertical flux of entropy from the boundary layer into the free troposphere. (We ignore the irreversible generation of entropy in our idealized models.) When this balance occurs the vertically integrated moist entropy remains approximately constant. In general, only a statistical balance is possible in moist RCE, since local entropy anomalies and subsequent convective episodes continually occur within the real and modeled atmosphere – though in the case of parameterized convection, moist RCE can take the form of a true steady state. It is thus a statistical equilibrium we seek in calculations of RCE in this study, and upon this state, perturbations are applied.

We obtain RCE states for each of the parameter sets described in Table 1 by initializing the model with prescribed values of the surface wind speed, lapse rate, relative humidity and tropopause height. The model is then run for 360 days with no applied perturbations. We use a column of 81 grid cells with a constant vertical resolution of $\Delta z = 250$ m. The sea surface temperature is set to a constant value of SST = 303 K and the imposed surface wind speed is 5 m/s. The model provides output every half-day and uses a time step of 300 s. Specific entropy profiles from such a calculation are shown in Figure 1. The kinks in the entropy profiles near 850 hPa are due to the different modes of convective adjustment applied to the boundary layer and the free troposphere.

A height-dependent fractional perturbation of either positive or negative sign is then applied to the initial potential temperature profile. Each perturbation is in the form of half of a second baroclinic mode, in that the anomaly is limited to either the upper or lower half (in the sense of geopotential height) of the troposphere and is in the shape of a sine function so that half the characteristic wavelength spans one half of the tropospheric depth (see Figure 2).

The model is then reinitialized with the modified profile and allowed to adjust over a 10 day period under the same forcing scheme used in the respective RCE experiment, only with a much shorter output period of 15 min. In this way, the model begins at the RCE state, except that its potential temperature profile is perturbed at the first time step. During the rest of the run, the model relaxes back to the RCE state it must achieve under the original forcing conditions.

The response behavior of the model is illustrated by three variables of interest: precipitation rate, specific moist entropy s and adiabatic warming j. The mechanisms changing these variables are different. As noted previously, specific moist entropy s, and the adiabatic warming j both change when diabatic heating or cooling occurs due to

Table 1. The Forcing Parameters Used and Mean Rainfall Rates Obtained in the Trials of the SCM and CRM Experiments.

Trial	Surface Drag Coefficient ($\times 10-3$)	Radiative Cooling Rate (K/day)	Mean RCE Rain Rate in SCM (mm/day)	Mean RCE Rain Rate in CRM (mm/day)
A	0.5	−1.0	2.2	2.0
B	1.0	−2.0	4.5	4.3
C	1.5	−3.0	6.6	7.1
D	2.0	−4.0	8.7	8.7
E	2.5	−5.0	10.8	10.8
F	3.0	−6.0	12.8	12.3

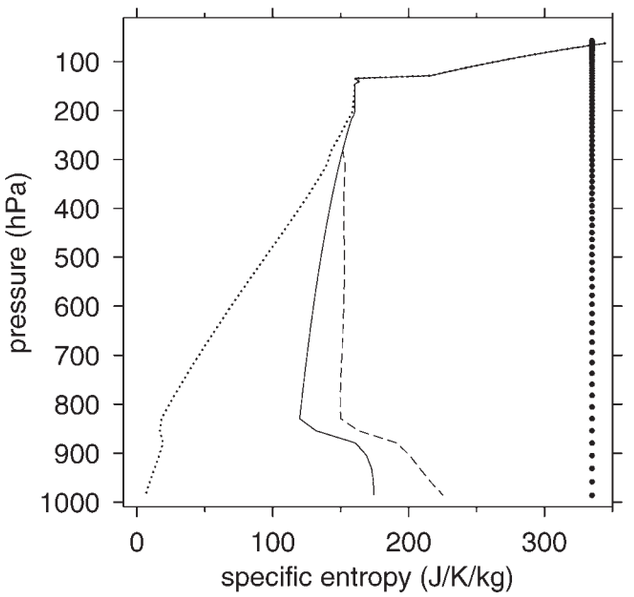

Figure 1. Specific entropy profiles for the averaged RCE calculation for Trial B of the SCM. Dry entropy (dotted), moist entropy (solid) and saturated moist entropy (dashed) are shown. The dots on the far right indicate the vertical grid spacing.

radiation or surface fluxes. In addition, the adiabatic warming j changes in response to condensation and evaporation.

The responses of these variables to cold anomalies at upper and lower elevations are illustrated in Figures 3 and 4, respectively. The plots in Figures 3 and 4 represent the time evolution over 3 hr of mass-weighted, column-integrated perturbations from the RCE state of s and j, resulting from the applied perturbation in potential temperature for each trial described in Table 1. In the upper troposphere, both variables have decreased from their initial, unperturbed values, since the temperature has been impulsively changed while leaving the mixing ratio unchanged. Following the impulse, both variables remain fairly constant, although the adiabatic warming increases slightly over the interval shown.

Unlike in the upper troposphere, the adiabatic warming in the lower troposphere increases quickly over the first two hours, leveling off somewhat thereafter. Since the moist entropy remains nearly constant over this interval, the warming is primarily due to condensation and latent heat release.

The model precipitation responses to warm and cold anomalies are illustrated for each trial in Figure 5. Precipitation behavior following the temperature perturbation is similar to that of the adiabatic warming; while rain responses to warming and cooling are nearly zero in all cases for the upper elevation perturbations, those following lower elevation perturbations are significant and are comparable to the mean rainfall rate for each respective set of forcing parameters (see Table 1). The asymmetry between rainfall perturbations in trials A, B and C results from lower mean rainfall rates in these cases, which limits the magnitude of negative perturbations.

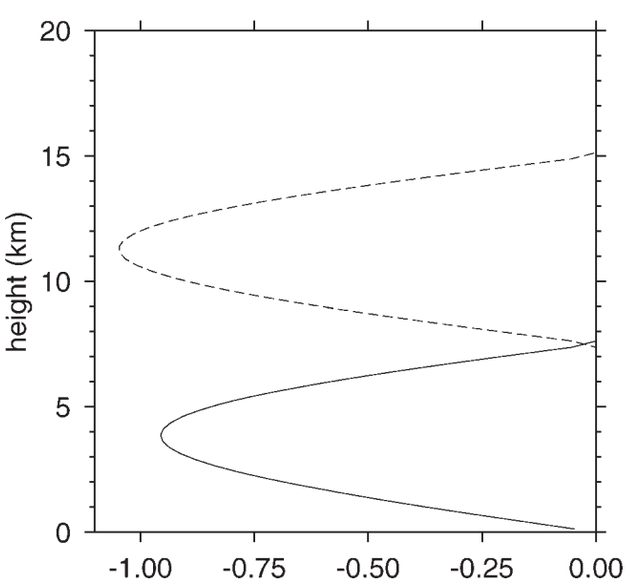

Figure 2. Profiles of negative potential temperature perturbations for upper (dashed line) and lower (solid line) elevation cases. The perturbation magnitudes were defined as fractions of the ambient potential temperature profile, which results in the slight difference in magnitude between the upper and lower perturbations.

4. Impulsive Heating in a Cloud-Resolving Model

In the previous section, a single-column toy model is used to show that temperature anomalies relax to an RCE state faster in the lower troposphere due to the amount of water vapor available there compared to layers aloft. In the current section, we test the same idea using a three-dimensional cloud-resolving model (CRM) using a technique similar to that employed by *Tulich and Mapes* [2010]. This is an important aspect of the study, because it serves as a stepping stone between the theoretical model expressed in the parameterization scheme of the SCM and the real atmosphere. To this end, increased stochastic behavior due to greater degrees of freedom help to imitate the capricious nature of the atmospheric fluid, while ensemble averaging used in this part of the study elicits dominant model characteristics. Since observations of subtle changes in the thermodynamic fields of the atmosphere are difficult to obtain in a form useful to this study, the CRM results described here provide evidence until definitive observational studies can better inform the hypothesis.

The CRM used in this study is similar to that described by *Raymond and Zeng* [2005] with minor changes made since that paper. The model integrates the non-rotating, fully compressible Navier-Stokes equations, mass continuity, and prognostic relations for equivalent potential

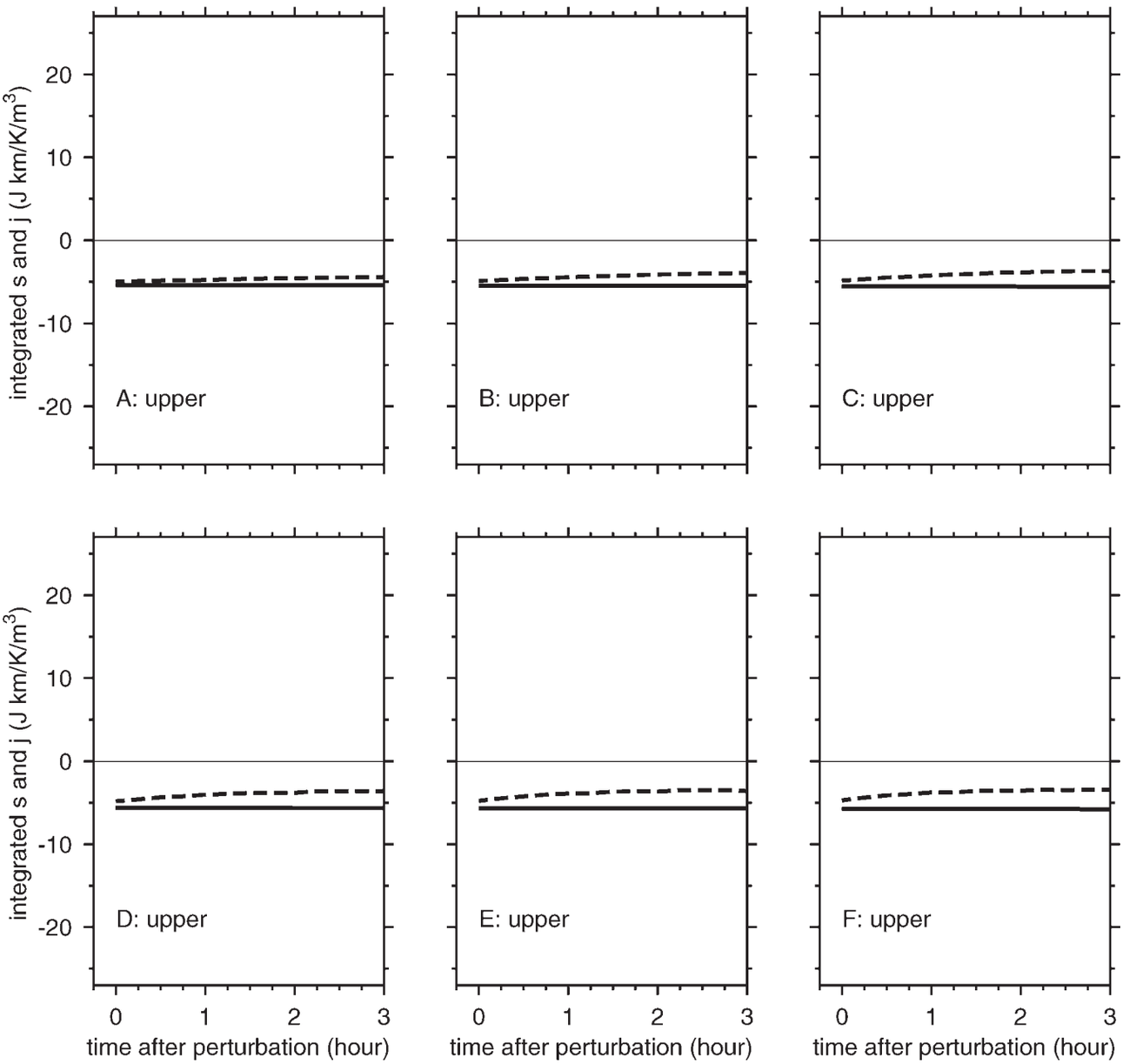

Figure 3. Recovery of mass-weighted, vertically integrated specific moist entropy (solid lines) and adiabatic warming (dashed lines) over 3 hour period following upper elevation cooling perturbations for each trial outlined in Table 1 for the SCM experiment. To simplify comparison, the vertical scales of these figures have been chosen to match those of Figures 4, 7, and 8.

temperature, total cloud water and precipitation mixing ratios. The radiative cooling scheme is identical to that of the SCM.

As in the SCM experiment described in section 3, an RCE calculation is first made for each combination of radiative cooling and surface drag coefficients shown in Table 1. To this end, under the respective forcing conditions, the model is run to statistical equilibrium (this requires a period of 30–60 days), which we take to represent the RCE state. The model uses a time step of $\Delta t = 0.5$ s and provides output every 10^4 s. We use the same vertical resolution, initial SST and column height as used in the SCM. The horizontal domain is bowling alley-shaped, with a grid spacing of $\Delta x =$ 1000 m. We use 160 and 15 points in the x and y dimensions, respectively. Since the model is parallelized along the x-dimension, 160 km was chosen as a multiple of the number of available processors and the overall domain size is a result of the familiar compromise between competing desires to maximize area and resolution while maintaining a tractable run time.

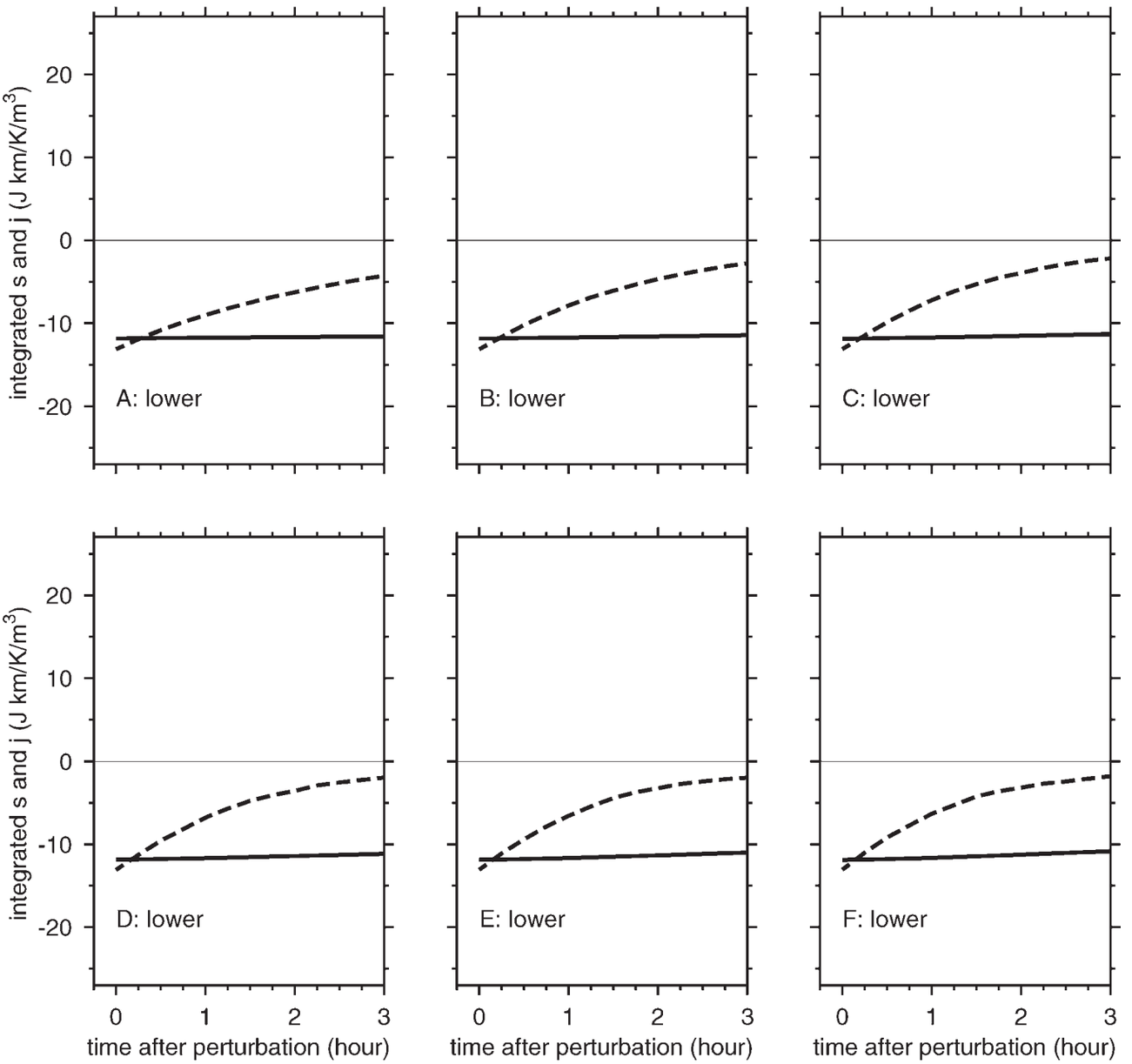

Figure 4. Same as Figure 3 but for lower elevation perturbations.

A horizontal resolution of 1000 m is insufficient to truly ''resolve'' a cumulonimbus cloud which might have updrafts of order 3000 – 5000 m in diameter. Some authors prefer the term ''cloud-permitting models'' rather than ''cloud-resolving models'' because of this. There is thus some uncertainty introduced into the results by the possibly insufficient resolution. However, computational limitations prevent us from addressing this issue at the present time.

Initialization profiles are time averages over the last 30 days of the RCE run. A typical set of domain-averaged entropy profiles for the RCE state is shown in Figure 6. Control and perturbation calculations for each trial are then made at a higher time resolution (output every 15 min) so that fine detail of the response can be observed.

When the model is re-initialized using the mean RCE profiles discussed above, there is some period of adjustment during which no rainfall occurs. This is the time over which boundary layer entropy anomalies attain buoyancies sufficient to initiate convection for the first time. Since rainfall happens on an almost continual basis (though at different locations within the domain) during a modeled RCE state, it is assumed that the model is not in RCE during this initial period. Thus, to ensure the model has returned to its equilibrium state, the prescribed perturbation tendencies

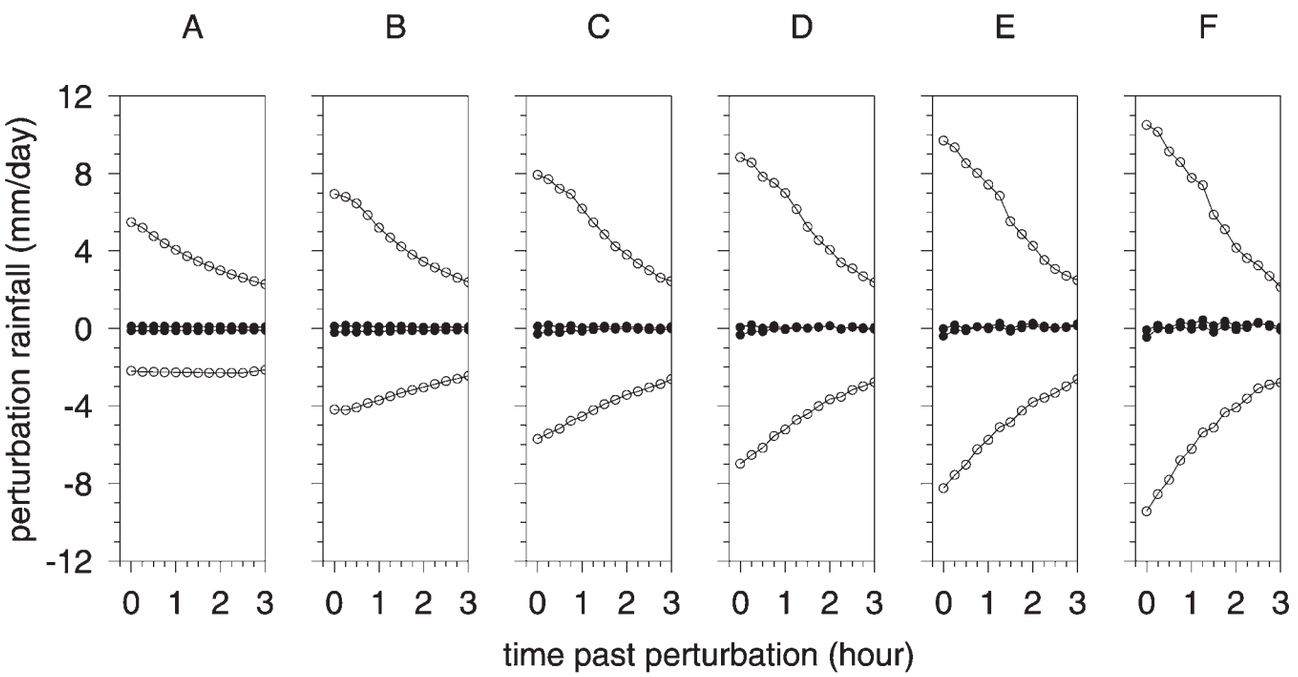

Figure 5. Rain response of SCM over first 3 hours following prescribed perturbations for each trial described in Table 1. The open circles above the zero axis in each plot represent the perturbation rainfall for lower elevation cooling perturbations, while those below zero illustrate the responses to lower elevation warming. The upper elevation warming and cooling responses are represented by the solid circles in each plot.

are not applied until this adjustment period is over. The length of this period differs for each trial according to the forcing strength defined by the respective radiative cooling and surface drag coefficients.

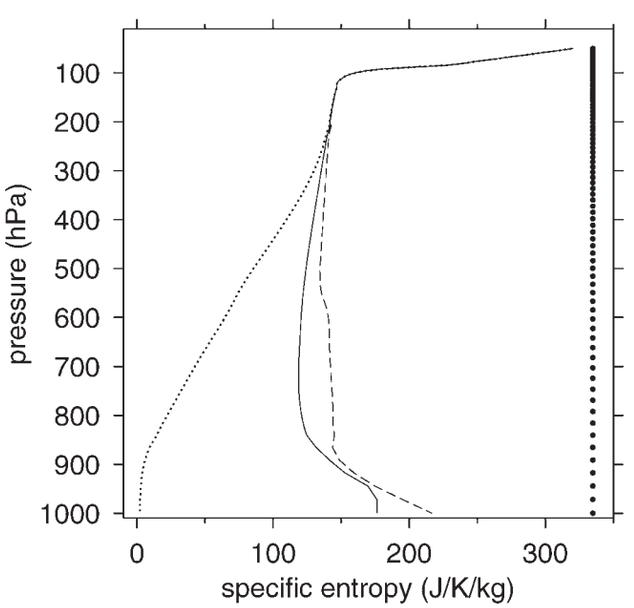

Figure 6. As in Figure 1 except the RCE calculation for the CRM.

The perturbation tendencies are applied to the potential temperature field in the manner of *Tulich and Mapes* [2010] in order to effect temperature perturbations similar to those applied to the SCM in section 3. Tendencies are applied to the full horizontal model domain and vary in the vertical as shown in Figure 2. The tendencies are applied over a 15 minute interval and are calculated such that the final temperature anomalies at the end of the interval are approximately ± 1 K. Each perturbation trial is performed as an ensemble of 16 runs over which the onset of prescribed tendencies are staggered. This is necessary since the response is highly dependent on the state of the model at the time of perturbation, an effect that is illustrated in Figure 10.

In order to analyze the results of the perturbation experiments in terms of CQE assumptions, we again examine aspects of the thermodynamic state of the model following temperature perturbations by comparing the RCE state, represented here by the control run for each trial, to the perturbed state. As the RCE state represents a statistical equilibrium, we take departures of the moist entropy and adiabatic warming from the RCE value to illustrate changes in the model. Lastly, since the adiabatic warming is primarily affected by moisture phase changes, we examine the rainfall.

The moist entropy and adiabatic warming responses following cooling perturbations are shown for the upper and lower elevation cases in Figures 7 and 8, respectively. As in Figures 3 and 4, the differences in these variables from

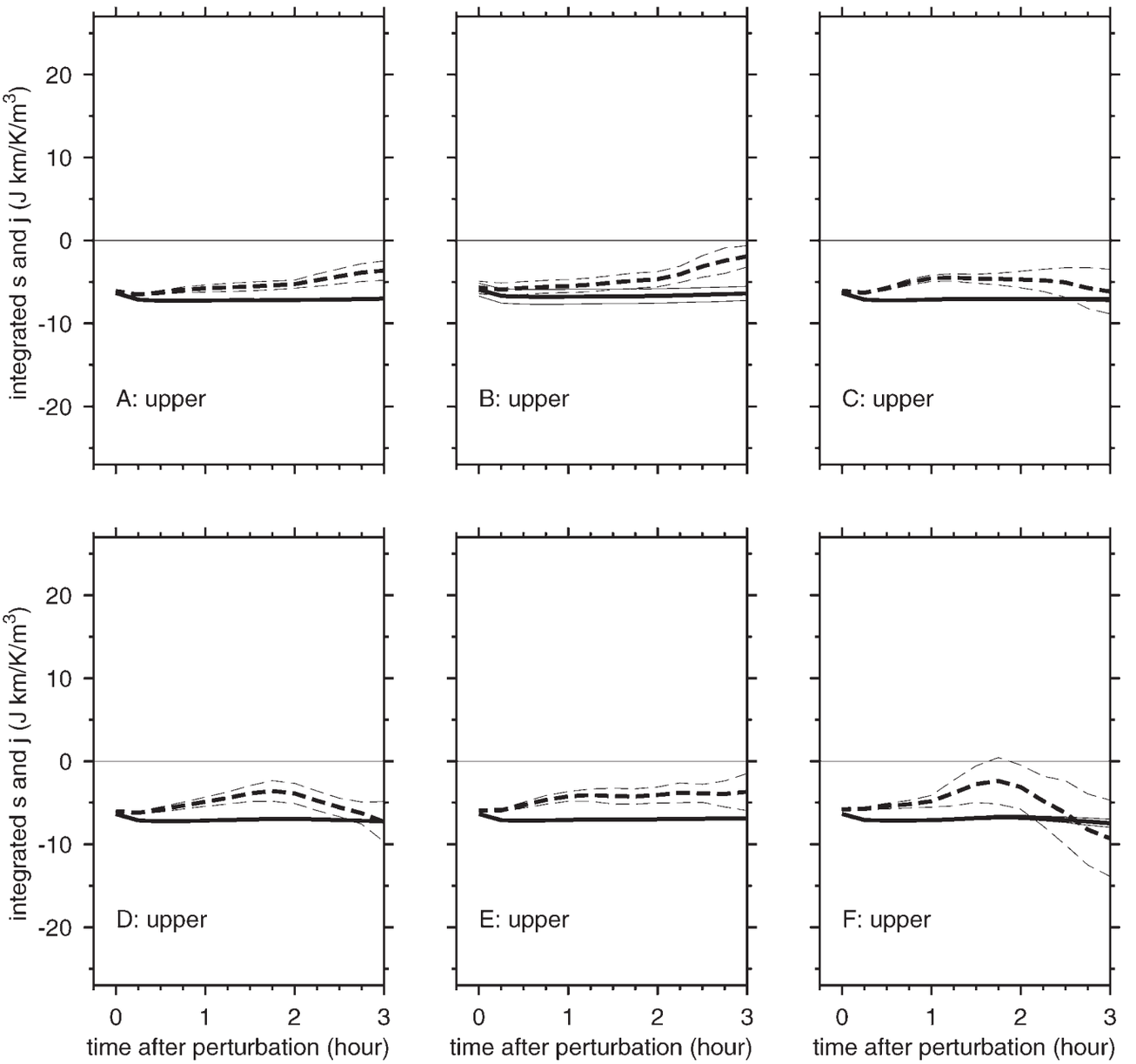

Figure 7. Same as Figure 3 but for the CRM. Both variables are ensemble means that have been domain averaged in the horizontal. The thin lines indicate 95% confidence intervals around the mean estimates.

those of the control run have been mass-weighted and column-integrated. Furthermore, the plots represent the domain-averaged ensemble mean for each of the forcing regimes shown.

As in the SCM experiment, both variables change slowly following upper elevation perturbations, though the adiabatic warming changes somewhat more rapidly than the entropy. Following lower elevation perturbations, the adiabatic warming reacts drastically, while the moist entropy remains nearly constant. The combined behavior of moist entropy and adiabatic warming following lower tropospheric cooling again signals the formation of condensate, which anticipates rain.

Plots of the rainfall response are shown in Figure 9. Each plot reveals the ensemble mean response following the applied perturbation in rainfall for the corresponding set of forcing parameters described in Table 1. Negative perturbations in temperature lead to positive rainfall anomalies and the response is far greater for lower-elevation perturbations; this trend is consistent throughout the range of forcing strengths. Unlike the SCM experiment, the rainfall response appears to be a weak function of the forcing

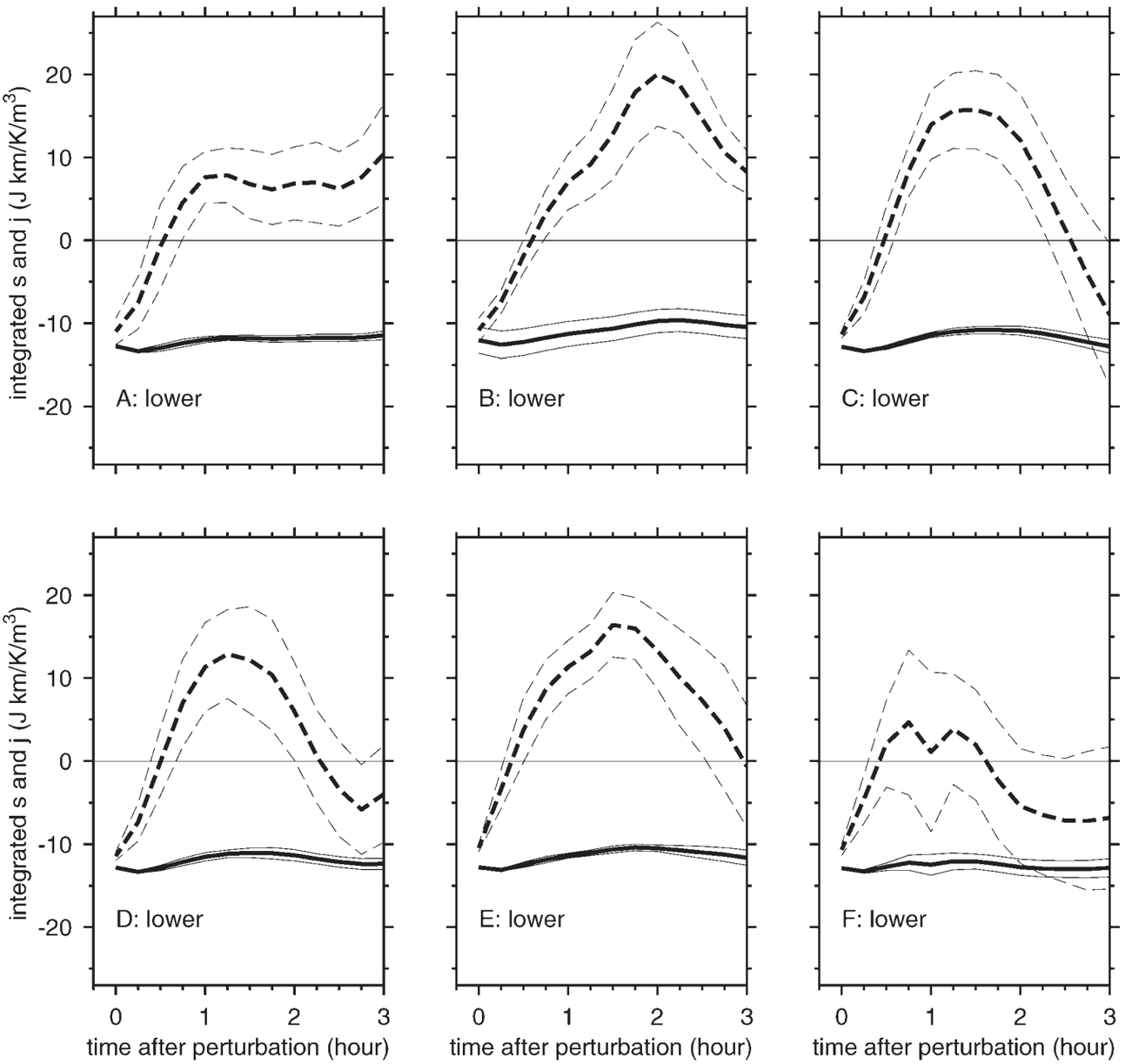

Figure 8. Same as Figure 7 but for lower elevation perturbations.

strength as the variation in anomalous rainfall is non-monotonic and irregular over the range of trials. The variation in response shown is likely due to the relatively small number of trials in each ensemble as well as to the small domain size, which permits only a few clouds at any one time. Both circumstances lead to greater expression of the stochastic variability across the spectrum of trials.

The variation in rainfall response over the members of a single ensemble lends credence to this idea and is illustrated in Figure 10. In this set of plots, the response for each run in the ensemble for Trial B is shown as a dotted line and the mean response across the ensemble is shown as a solid line. Individual runs show a high degree of variation suggesting that only gross features are robust. As in the SCM case, the rainfall response to heating and cooling is asymmetric, though the details are different.

5. Conclusions

Convective quasi-equilibrium in the sense of ENB is the hypothesis that convection forces the atmospheric temperature profile to a form governed only by the boundary layer moist entropy. If true, this hypothesis simplifies large-scale dynamics in convectively active regions by greatly reducing the number of degrees of freedom available to the dynamical evolution of the atmosphere.

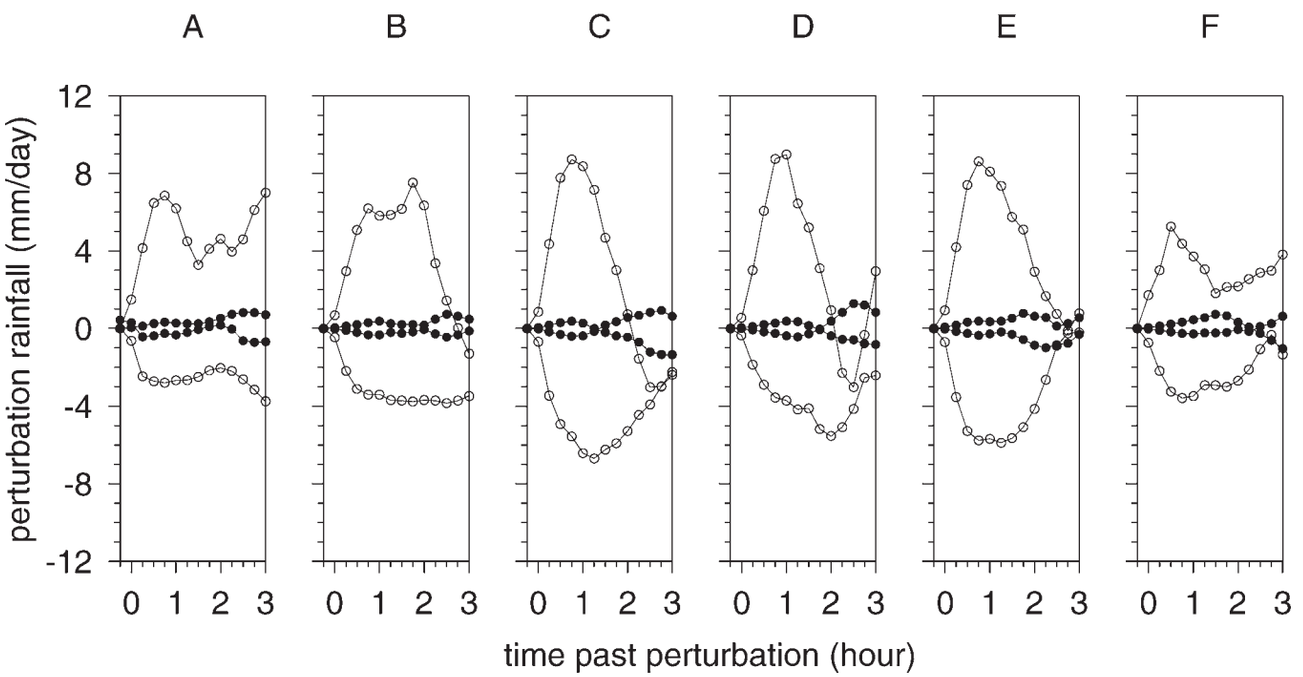

Figure 9. As in Figure 5 but for the CRM trials. Each plot represents the ensemble mean for each trial.

Though appealing in its simplicity, we assert that (1) the adiabatic warming rather than the temperature is the appropriate adjustment variable in moist convective quasi-equilibrium, and (2) the quasi-equilibrium hypothesis is only valid in roughly the lower half of the troposphere. The adjustment problem could be couched in terms of the temperature alone, as has been customary. However, in rapid adjustment the moist entropy is nearly conserved, which means that for each rapid adjustment in temperature there is a corresponding rapid adjustment in moisture of the opposite sign. Thinking of the two-dimensional abstract space with axes $C_p \ln \theta$ and Lr/T_R, the adiabatic warming j and the moist entropy s define coordinate axes rotated $-45°$ from the original axes, as illustrated in Figure 11. Rapid adjustment may be viewed as motion in this space parallel to the j axis, while slow adjustment is motion parallel to the s axis.

The quasi-equilibrium hypothesis as it is currently expressed by ENB is silent regarding moisture adjustment. This is a major omission given the role of moisture and the production of precipitation in deep convection. Our treatment in terms of s and j makes it clear that rapid adjustment in moisture goes hand in hand with rapid adjustment in temperature. This adjustment results from phase changes of water substance. All variations having to do with phase changes are concentrated in one variable, the adiabatic warming; the moist entropy remains constant under changes of phase and typically changes only slowly under the influence of radiation and heat conduction from the surface. Precipitation production occurs on the convective time scale and is the origin of the rapid thermodynamic transformations needed for moist convective quasi-equilibrium to work.

Precipitation production is concentrated in the lower troposphere since most of the water vapor is concentrated there. This suggests that the changes in thermodynamic state needed for convective adjustment operate much more rapidly in the lower troposphere than in the upper troposphere.

To test this hypothesis, we conducted a series of numerical experiments with a physically based toy cumulus parameterization in SCM mode and a cloud-resolving model. In both cases a computational domain initially in radiative-convective equilibrium is subjected to a perturbation in the temperature profile. The rapidity with which convection subsequently adjusts the mean profile of adiabatic warming back to equilibrium is much greater in the lower troposphere than in the upper troposphere. At upper levels the adjustment rate of adiabatic warming differs only modestly from the slow response of moist entropy. Thus, the convective quasi-equilibrium hypothesis appears to be valid in the lower troposphere but not in the upper troposphere. These forward computations confirm the results of *Tulich and Mapes* [2010] and those of *Kuang* [2010] obtained by his inverse calculation method. Furthermore, *Kuang*'s [2010] rapidly decaying eigenmodes appear to be primarily associated with perturbations in adiabatic warming j, while the more slowly decaying modes are composed mainly of perturbations in moist entropy s.

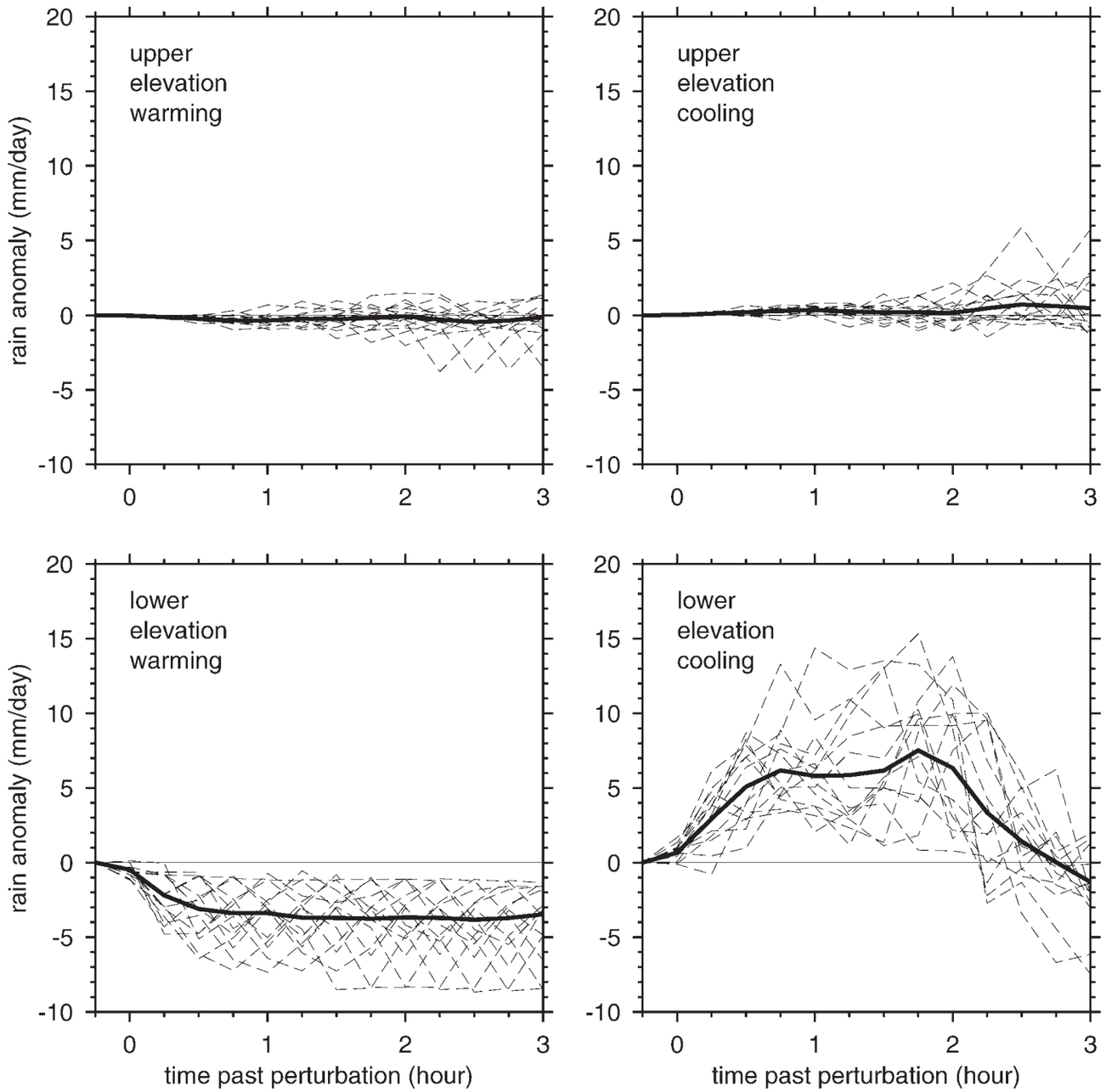

Figure 10. Precipitation response of 16 ensemble runs for (top) upper and (bottom) lower elevation perturbations for Trial B of the CRM experiment. The individual responses of each run are shown as thin dotted lines and the thick solid line shows the ensemble mean. The zero axis is indicated by a thin solid line in each plot.

The most important consequence of this result is that the upper tropospheric part of the adiabatic warming profile has much more freedom to vary under the influence of large-scale dynamics than does the lower tropospheric part, which is strongly constrained by cumulus convection in convectively active regions. This has significant dynamical consequences for large-scale tropical flows, as discussed by *Kuang* [2010] and in section 1. Dynamical models employing cumulus parameterizations which invoke full-tropospheric convective quasi-equilibrium in the sense of ENB are unlikely to produce results in accord with observation.

Acknowledgments: The seeds of this work were sown at a workshop organized by Zhiming Kuang as a result of work presented there by Brian Mapes and Stefan Tulich. We thank Kerry Emanuel and Zhiming Kuang for helpful reviews of this paper. This research was supported by National Science Foundation grant ATM-1021049 and

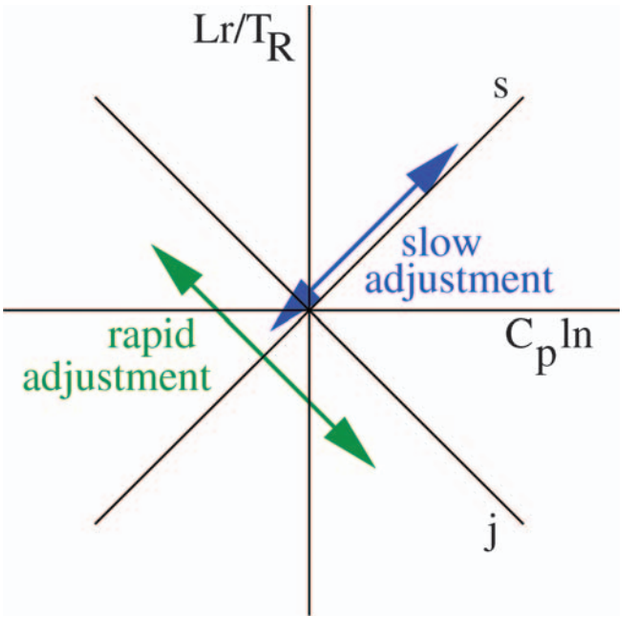

Figure 11. Illustration of slow and rapid adjustments in the C_p ln $\theta - Lr/T_R$ plane. The moist entropy *s* and adiabatic warming *j* axes are rotated −45° from the original axes.

Office of Naval Research grant N00014-08-1-0241. The CRM simulations were performed using the Encanto supercomputer, a resource of the New Mexico Computing Applications Center. The graphics were made with Dan Kelley's GRI Graphing Language.

References

Arakawa, A., and W. H. Schubert 1974, Interaction of a cumulus cloud ensemble with the large-scale environment, part I, *J. Atmos. Sci.*, **31**, 674–701, doi: 10.1175/1520-0469(1974)031<0674:IOACCE>2.0.CO;2.

Betts, A. K. 1986, A new convective adjustment scheme. Part I: Observational and theoretical basis, *Q. J. R. Meteorol. Soc.*, **112**, 677–691.

Betts, A. K., and M. J. Miller 1986, A new convective adjustment scheme. Part II: Single column tests using GATE wave, BOMEX, ATEX and arctic air-mass data sets, *Q. J. R. Meteorol. Soc.*, **112**, 693–709.

Betts, A. K., and M. J. Miller 1993, The Betts-Miller scheme, *The Representation of Cumulus Convection in Numerical Models,* edited by K. A. Emanuel and D. J. Raymond, pp. 107–121, Am. Meteorol. Soc., Boston, Mass

Emanuel, K. A. 1995, The behavior of a simple hurricane model using a convective scheme based on subcloud-layer entropy equilibrium, *J. Atmos. Sci.*, **52**, 3960–3968, doi: 10.1175/1520-0469(1995)052<3960:TBOASH>2.0.CO;2.

Emanuel, K. A., J. D. Neelin, and C. S. Bretherton 1994, On large-scale circulations in convecting atmospheres, *Q. J. R. Meteorol. Soc.*, **120**, 1111–1143, doi: 10.1002/qj.49712051902.

Frierson, D. M. W. 2007, Convectively coupled Kelvin waves in an idealized moist general circulation model, *J. Atmos. Sci.*, **64**, 2076–2090, doi: 10.1175/JAS3945.1.

Frierson, D., D. Kim, I.-S. Kang, M.-I. Lee, and J. Lin 2011, Structure of AGCM-simulated convectively coupled Kelvin waves and sensitivity to convective parameterization, *J. Atmos. Sci.*, **68**, 26–45, doi: 10.1175/2010JAS3356.1.

Khouider, B., and A. J. Majda 2006, A simple multicloud parameterization for convectively coupled tropical waves. Part I: Linear analysis, *J. Atmos. Sci.*, **63**, 1308–1323, doi: 10.1175/JAS3677.1.

Khouider, B., and A. J. Majda 2008, Multicloud models for organized tropical convection: Enhanced congestus heating, *J. Atmos. Sci.*, **65**, 895–914, doi: 10.1175/2007JAS2408.1.

Kiladis, G. N., M. C. Wheeler, P. T. Haertel, K. H. Straub, and P. E. Roundy 2009, Convectively coupled equatorial waves, *Rev. Geophys.*, **47**, RG2003, , doi: 10.1029/2008RG000266

Kuang, Z. 2008a, Modeling the interaction between cumulus convection and linear gravity waves using a limited-domain cloud system-resolving model, *J. Atmos. Sci.*, **65**, 576–591, doi: 10.1175/2007JAS2399.1.

Kuang, Z. 2008b, A moisture-stratiform instability for convectively coupled waves, *J. Atmos. Sci.*, **65**, 834–854, doi: 10.1175/2007JAS2444.1.

Kuang, Z. 2010, Linear response functions of a cumulus ensemble to temperature and moisture perturbations and implications for the dynamics of convectively coupled waves, *J. Atmos. Sci.*, **67**, 941–962, doi: 10.1175/2009JAS3260.1.

Lee, M.-I., I.-S. Kang, and B. E. Mapes 2003, Impacts of cumulus convection parameterization on aqua-planet AGCM simulations of tropical intraseasonal variability, *J. Meteorol. Soc. Jpn.*, **81**, 963–992, doi: 10.2151/jmsj.81.963.

Majda, A. J., and J. A. Biello 2004, A multi-scale model for tropical intraseasonal oscillations, *Proc. Natl. Acad. Sci. U. S. A.*, **101**, 4736–4741, doi: 10.1073/pnas.0401034101.

Majda, A. J., and M. G. Shefter 2001, Models for stratiform instability and convectively coupled waves, *J. Atmos. Sci.*, **58**, 1567–1584, doi: 10.1175/1520-0469(2001)058<1567:MFSIAC>2.0.CO;2.

Mapes, B. E. 2000, Convective inhibition, subgrid-scale triggering energy, and stratiform instability in a toy tropical wave model, *J. Atmos. Sci.*, **57**, 1515–1535, doi: 10.1175/1520-0469(2000)057<1515:CISSTE>2.0.CO;2.

Moorthi, S., and M. J. Suarez 1992, Relaxed Arakawa-Schubert: A parameterization of moist convection for general circulation models, *Mon. Weather Rev.*, **120**, 978–1002, doi: 10.1175/1520-0493(1992)120<0978:RASAPO>2.0.CO;2.

Neelin, J. D., and I. M. Held 1987, Modeling tropical convergence based on the moist static energy budget, *Mon. Weather Rev.*, **115**, 3–12, doi: 10.1175/1520-0493(1987)115<0003:MTCBOT>2.0.CO;2.

Neelin, J. D., and J.-Y. Yu 1994, Modes of tropical variability under convective adjustment and the Madden-Julian oscillation. Part I: Analytical theory, *J. Atmos. Sci.*, **51**, 1876–1894, doi: 10.1175/1520-0469(1994)051<1876:MOTVUC>2.0.CO;2.

Pan, D.-M., and D. A. Randall 1998, A cumulus parameterization with a prognostic closure, *Q. J. R. Meteorol. Soc.*, **124**, 949–981.

Randall, D. A., and D.-M. Pan 1993, Implementation of the Arakawa-Schubert cumulus parameterization with a prognostic closure, in *The Representation of Cumulus Convection in Numerical Models*, edited by K. A. Emanuel and D. J. Raymond, pp. 137–144, Am. Meteorol. Soc., Boston, Mass

Raymond, D. J. 1995, Regulation of moist convection over the west Pacific warm pool, *J. Atmos. Sci.*, **52**, 3945–3959, doi: 10.1175/1520-0469(1995)052<3945:ROMCOT>2.0.CO;2.

Raymond, D. J. 2007, Testing a cumulus parametrization with a cumulus ensemble model in weak-temperature-gradient mode, *Q. J. R. Meteorol. Soc.*, **133**, 1073–1085, doi: 10.1002/qj.80.

Raymond, D. J., S. Sessions, A. Sobel, and Ž. Fuchs 2009, The mechanics of gross moist stability, *J. Adv. Model. Earth Syst.*, **1**, 9, , doi: 10.3894/JAMES.2009.1.9

Raymond, D. J., and Ž. Fuchs 2007, Convectively coupled gravity and moisture modes in a simple atmospheric model, *Tellus, Ser. A*,**59**, 627–640.

Raymond, D. J., and X. Zeng 2005, Modelling tropical atmospheric convection in the context of the weak temperature gradient approximation, *Q. J. R. Meteorol. Soc.*, **131**, 1301–1320, doi: 10.1256/qj.03.97.

Straub, K. H., and G. N. Kiladis 2002, Observations of a convectively coupled Kelvin wave in the eastern Pacific ITCZ, *J. Atmos. Sci.*, **59**, 30–53, doi: 10.1175/1520-0469(2002)059<0030:OOACCK>2.0.CO;2.

Sud, Y. C., and G. K. Walker 1999a, Microphysics of clouds with the relaxed Arakawa-Schubert scheme (McRAS). Part I: Design and evaluation with GATE phase III data, *J. Atmos. Sci.*, **56**, 3196–3220, doi: 10.1175/1520-0469(1999)056<3196:MOCWTR>2.0.CO;2.

Sud, Y. C., and G. K. Walker 1999b, Microphysics of clouds with the relaxed Arakawa-Schubert scheme (McRAS). Part II: Implementation and performance in GEOS II GCM, *J. Atmos. Sci.*, **56**, 3221–3240, doi: 10.1175/1520-0469(1999)056<3221:MOCWTR>2.0.CO;2.

Tokioka, T., K. Yamazaki, A. Kitoh, and T. Ose 1988, The equatorial 30–60 day oscillation and the Arakawa-Schubert penetrative cumulus parameterization, *J. Meteorol. Soc. Jpn.*, **66**, 883–901.

Tompkins, A. M., and G. C. Craig 1998, Time-scales of adjustment to radiative-convective equilibrium in the tropical atmosphere, *Q. J. R. Meteorol. Soc.*, **124**, 2693–2713.

Tulich, S., and B. Mapes 2010, Transient environmental sensitivities of explicitly simulated tropical convection, *J. Atmos. Sci.*, **67**, 923–940, doi: 10.1175/2009JAS3277.1.

Yang, G.-Y., B. Hoskins, and J. Slingo 2007, Convectively coupled equatorial waves. Part I: Horizontal and vertical structures, *J. Atmos. Sci.*, **64**, 3406–3423, doi: 10.1175/JAS4017.1.

Yano, J.-I., W. W. Grabowski, G. L. Roff, B. E. Mapes 2000, Asymptotic approaches to convective quasi-equilibrium, *Q. J. R. Meteorol. Soc.*, **126**, 1861–1887, doi: 10.1256/smsqj.56615.

Zhang, G. J. 2002, Convective quasi-equilibrium in mid-latitude continental environment and its effect on convective parameterization, *J. Geophys. Res.*, **107**D14, 4220, doi: 10.1029/2001JD001005